COMMUNICATIONS PHYSICS

ARTICLE

https://doi.org/10.1038/s42005-020-0294-6 OPEN

Adaptive optical beam steering and tuning system based on electrowetting driven fluidic rotor

Weifeng Cheng[1], Jiansheng Liu[2], Zheng Zheng[2], Xukun He[1], Bowen Zheng[3], Hualiang Zhang[3], Huachen Cui[1], Xiaoyu Zheng[1], Tao Zheng[4], Bruce E. Gnade[4] & Jiangtao Cheng[1*]

Reconfigurable beam steering components are indispensable to support optical and photonic network systems operating with high adaptability and with various functions. Currently, almost all such components are made of solid parts whose structures are rigid, and hence their functions are difficult to be reconfigured. Also, optical concentration beam steering is still a very challenging problem compared to radio frequency/microwave steering. Here we show a watermill-like beam steering system that can adaptively guide concentrating optical beam to targeted receivers. The system comprises a liquid droplet actuation mechanism based on electrowetting-on-dielectric, a superlattice-structured rotation hub, and an enhanced optical reflecting membrane. The specular reflector can be adaptively tuned within the lateral orientation of 360°, and the steering speed can reach ~353.5° s^{-1}. This work demonstrates the feasibility of driving a macro-size solid structure with liquid microdroplets, opening a new avenue for developing reconfigurable components such as optical switches in next-generation sensor networks.

[1] Department of Mechanical Engineering, Virginia Polytechnic Institute and State University, Blacksburg, VA 24061, USA. [2] School of Electronic and Information Engineering, Beihang University, 37 Xueyuan Road, Haidian District, Beijing 100191, China. [3] Department of Electrical and Computer Engineering, University of Massachusetts Lowell, Lowell, MA 01854, USA. [4] Department of Mechanical Engineering, Southern Methodist University, Dallas, TX 75205, USA. *email: chengjt@vt.edu

During the past two decades, the development of multi-functional sensing networks, swift signal transmission systems, and advanced wireless communication techniques has grown rapidly. Their applications are ubiquitous in our daily lives, ranging from optical switches[1–3], laser beam security networks[4], in-home WiFi antenna networks[5], global positioning systems (GPS)[6] to autonomous vehicle remote control[7]. To make these advanced sensing and telecommunication networks feasible in a more complex environment, a higher level of beam signal transmission standards, e.g., avoidance of signal mitigation over a longer transmission distance and alleviation of the multi-path fading phenomenon, needs to be carefully addressed. In this regard, adaptive beam steering technology has been highly demanded as it can effectively guide the concentrating beams to the desired paths and protect the network from noise disturbance.

Compared with radio frequency (RF)/microwave beam steering via various antenna techniques, optical beam steering is still a very challenging problem. A high-performance optical beam steering system with comprehensive merits such as low insertion loss, fast steering speed, wide steering range, high steering resolution, less system complexity, and compact platform size is highly demanded. During recent years, several novel fluid-based beam tuning mechanisms have been developed especially for optical beam steering. Among them, the beam tuning system driven by electrowetting on dielectric (EWOD)[8–10], which is defined as the change in the contact angle between an electrolyte and a dielectric surface owing to an applied electric potential between them, shows distinct advantages. EWOD-based digital operations[11] have demonstrated great potential in actuating and manipulating liquid droplets owing to EWOD's unique characteristics of prompt response (tens of ms), low power consumption (μW—mW), and programmable operations. Based on EWOD, tunable liquid prisms can reflect incident beams to the desired direction by controlling the orientation of a reflecting membrane located on a droplet surface or embedded at a fluid–fluid interface[12–17]. The maximum tilting angle among these tunable prism configurations has reached ~22°[18]. As a comparison, a functional dielectrophoresis-driven liquid prism was shown to steer beams only within ±0.87°[19]. Furthermore, a liquid–liquid light steering device actuated by dielectrowetting was developed and its maximum beam steering angle can reach ±22.7°[20]. In addition to the liquid prism-based steering mechanism, an EWOD-driven rotating shaft device was developed to modulate a membrane reflector within a range of ±30°[21], indicative of an apparent improvement over the liquid prism modules. Generally, liquid-based beam tilting and steering systems driven by EWOD require high stability of the fluid–fluid interface or the bulk fluids. In this respect, modulation of the embedded reflector at the fluid–fluid interface usually has a relatively low stability and is consequently hard to achieve full-range tracking and agile steering. Therefore, tuning devices capable of achieving fast, stable, and accurate responses for adaptive and wide range beam steering are still desired.

Inspired by capillary rotors with annular-shaped electrode designs[15], we put forward an optical concentrating beam steering system based on EWOD. The whole system comprises an annular EWOD platform with an open-plate configuration, a superlattice-structured rotation hub, and an enhanced optical reflecting membrane attached to the hub as the beam reflector. The EWOD platform is fabricated by sequentially depositing an annular array of Au electrodes, a thin film of Si_3N_4 dielectric, and a thin layer of hydrophobic fluoropolymer on a glass substrate. The rotary hub is made of silicone oxycarbide (SiOC) ceramic with an octet-truss superlattice structure of ultralight weight (~8 mg), ultrahigh strength (9 MPa) and ultrahigh stiffness (950 MPa), which is additively manufactured by scanning optics projection micro-stereolithography (SOPμSL)[22]. A low frequency alternative current (AC) voltage is applied to actuate a liquid microdroplet via EWOD along the annular loop to activate the specular reflector, to which the liquid droplet is adhered. A resistor-capacitor (RC) circuit network analysis of the EWOD system indicates that the EWOD driving force is in the order of hundreds of μN and its power consumption is ~10^{-5}–10^{-4} W. As such, the annular array of EWOD electrodes can be programmably activated to circulate a liquid droplet for digitally actuating the membrane reflector. Importantly, this EWOD-driven "watermill" is able to laterally rotate the reflector by 360° without the constraint of contact angle saturation[23–25], which outperforms most existing liquid-based actuation devices reported in the literature[12–16,19,21].

In this paper, the general setup of the rotary EWOD steering system and the fabrication of the superlattice hub are first introduced; then, a theoretical analysis of the EWOD driving force and the resistant force are discussed for feasibility validation. At last, the adaptive optical beam tuning on the rotary EWOD system is experimentally demonstrated. In particular, the testing results of optical beam steering range, tuning speed, beam tuning repeatability, and the specular reflectance of the reflector are reported.

Results

Superlattice rotary hub design. The overall EWOD-based optical beam steering system consists of an annular EWOD substrate, a rotational hub, and a reflecting membrane as shown in Fig. 1a. The adaptive beam steering is achieved by tuning the reflecting membrane through the EWOD-actuated liquid droplet. To enable smooth and facile rotation of the reflecting membrane, the 3D printed superlattice structure as illustrated in Fig. 1b was adopted as the rotary hub with ultralow weight and superior mechanical properties. Thus, a stretch-dominated cellular structure of the octet-truss superlattice[26,27] was fabricated using the SOPμSL system as shown in Fig. 1c[28,29], which is capable of fabricating large-volume, high-resolution complex superlattice structures. The ultraviolet (UV)-curable siloxane resin was formulated based on previous work[28] and was added into the resin bath to form the pre-ceramic parts. The 3D hub design was sliced into a sequence of 2D patterns, which were sequentially transmitted to a spatial light modulator and were illuminated with UV light from a light-emitting diode (LED) array. The exposed resin formed a cured layer imaging the shape of the 2D slice, and then the z axis elevator was lowered to recoat a thin film of the liquid resin for the subsequent 2D slice exposure. The 2D image projection step was then repeated to form the whole 3D structures as designed. Pre-ceramic parts were subsequently pyrolyzed in a tube furnace at 1000 °C with ultrahigh-purity Argon gas to form the superlatticed SiOC ceramic, as shown in Fig. 1d, e.

The relative density, $\bar{\rho}$, of the octet-truss lattice can be calculated as $\bar{\rho} = 6\sqrt{2}\left(\frac{b}{l}\right)^2$, where b is the strut thickness of the lattice and l is the node-to-node length. Therefore, the relative density of the as-formed lattice structure is 14%. Based on the volume of the hub (~24 mm^3) and the density of the base material (2.2 g cm^{-3} for SiOC), the weight of the latticed hub is ~7.4 mg. The strength of the hub $\sigma_{eff} \sim \alpha\bar{\rho}\sigma_s$ and its stiffness $E_{eff} \sim \beta\bar{\rho}E_s$, where σ_s and E_s are the strength and the Young's modulus of SiOC, respectively; α and β are pre-factors[30]. Therefore, the superlatticed rotary hub printed by SOPμSL has a high strength $\sigma_{eff} = 9$ MPa and an ultrahigh stiffness $E_{eff} = 950$ MPa.

Electrowetting driving force and resistant force analyses. The EWOD driving force versus the resistant force, which mainly includes the hub-shaft rotating friction and the droplet liquid-substrate friction, were analyzed to verify the feasibility of the

droplet actuation. In this work, an AC voltage was applied to manipulate the droplet transport as it can effectively mitigate dielectric polarization and prevent liquid electrolysis, as demonstrated in our previous work[31]. To analyze the EWOD driving force, a water droplet straddling two electrodes on the EWOD platform as shown in Fig. 2a, b was studied. Each trapezoidal electrode element with teeth (as shown in Supplementary Fig. 1 and Supplementary Note 1) is simplified as a sector-shaped unit in this analysis. One of the co-planar electrodes was activated with the leading edge of the droplet formed on it, and the adjacent electrode was assigned as the ground. Phenomenologically, the electrostatic energy stored in the dielectric layer under the droplet leads to a change in the apparent contact angle, inducing electrohydrodynamic force inside the droplet to drive it toward the activated electrode. On the other hand, the EWOD driving force can be analyzed via the lumped-parameter method based on an equivalent RC circuit of the EWOD system[32] as shown in Fig. 2a.

The area of the droplet on the actuated electrode, A_a, and that on the grounded electrode, A_g, can be determined by the droplet position angle θ, which is formed between the center of the droplet and the gap of the two electrodes. As illustrated in Fig. 2b, A_a and A_g are calculated as:

$$A_a(\theta) = \frac{2\cos^{-1}\left(\frac{R\sin\theta}{r}\right)}{2} r^2 - R\sin\theta \cdot r \cdot \sin\left(\frac{2\cos^{-1}\left(\frac{R\sin\theta}{r}\right)}{2}\right) \quad (1)$$

$$A_g(\theta) = \pi r^2 - A_a(\theta) \quad (2)$$

where r is the droplet radius and R is its radial distance from the shaft. In the lumped-parameter method, each dielectric part including the water droplet itself is considered as a RC component or RC group. For the co-planar configuration of EWOD, the RC circuit model consists of five RC components connected in series as shown in Fig. 2a. The resistances and capacitances of each RC component, which are dependent of A_a and A_g, are needed in order to calculate the equivalent total capacitance of the RC network (Supplementary Note 2 and parameter data are given in Supplementary Table 1).

The five RC groups are connected in series, so the total impedance Z_{tot} is the summation of the impedances of five components (Z_{fg}, Z_{fa}, Z_{sg}, Z_{sa}, and Z_w):

$$Z_{tot} = Z_{fg} + Z_{fa} + Z_{sg} + Z_{sa} + Z_w = \frac{1}{R_{tot} + \frac{1}{j\omega C_{tot}}} \quad (3)$$

By expressing the total impedance Z_{tot} with the capacitances and resistances of each component, the equivalent total capacitance of the RC network, C_{tot}, can be derived. With the value of C_{tot} and Z_{tot} obtained, the total electrostatic energy stored in the RC network $E = \frac{1}{2} C_{tot} V_{RMS}^2$ and the power consumption of the EWOD system $P_{tot} = \frac{V_{RMS}^2}{Z_{tot}}$ can be estimated, where $V_{RMS} = \frac{1}{2} V_{pk-pk}$ is the root-mean square of the applied square-wave AC voltage, and V_{pk-pk} is the peak to peak voltage referring to the amplitude of the square wave. We applied $V_{pk-pk} = 40$ V at 20 Hz in the experimental tests, so $V_{RMS} = 20$ V in the force analysis. Therefore, the electrostatic energy stored in the system increases with the square of the applied voltage magnitude. As the equivalent total capacitance is a function of the droplet position angle θ, which is formed between the droplet centroid and the electrode gap, and the angular frequency ω of the AC voltage, i.e., $C_{tot} \sim f(\theta, \omega)$, the EWOD driving force on the droplet can be calculated by taking the derivative with respect to θ, i.e.,

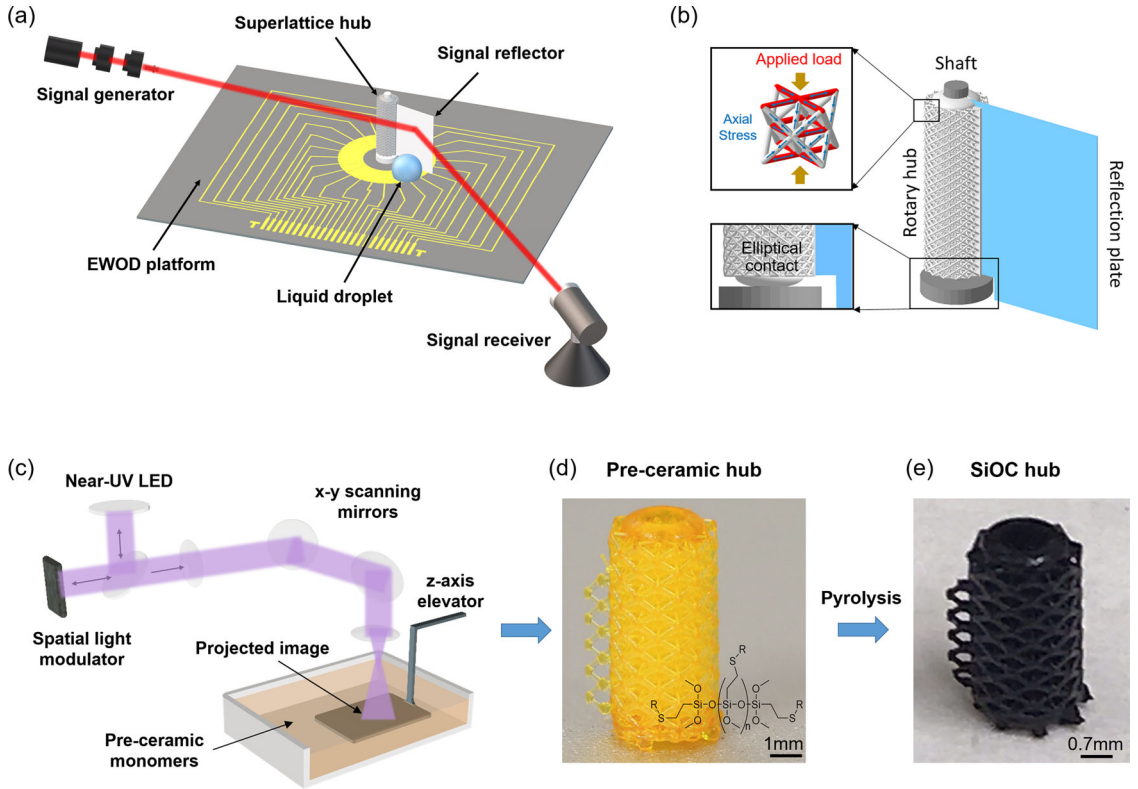

Fig. 1 Schematic of rotary electrowetting on dielectric (EWOD) optical beam steering system. a The assembled EWOD rotor system. **b** The superlattice hub design with elliptical contact on the base. **c** The scanning optics projection micro-stereolithography (SOPμSL) system[28]. **d** The pre-ceramic hub. **e** The pyrolyzed silicone oxycarbide (SiOC) hub. The SOPμSL system is employed for reducing the weight of the hub while maintaining its ultrahigh stiffness.

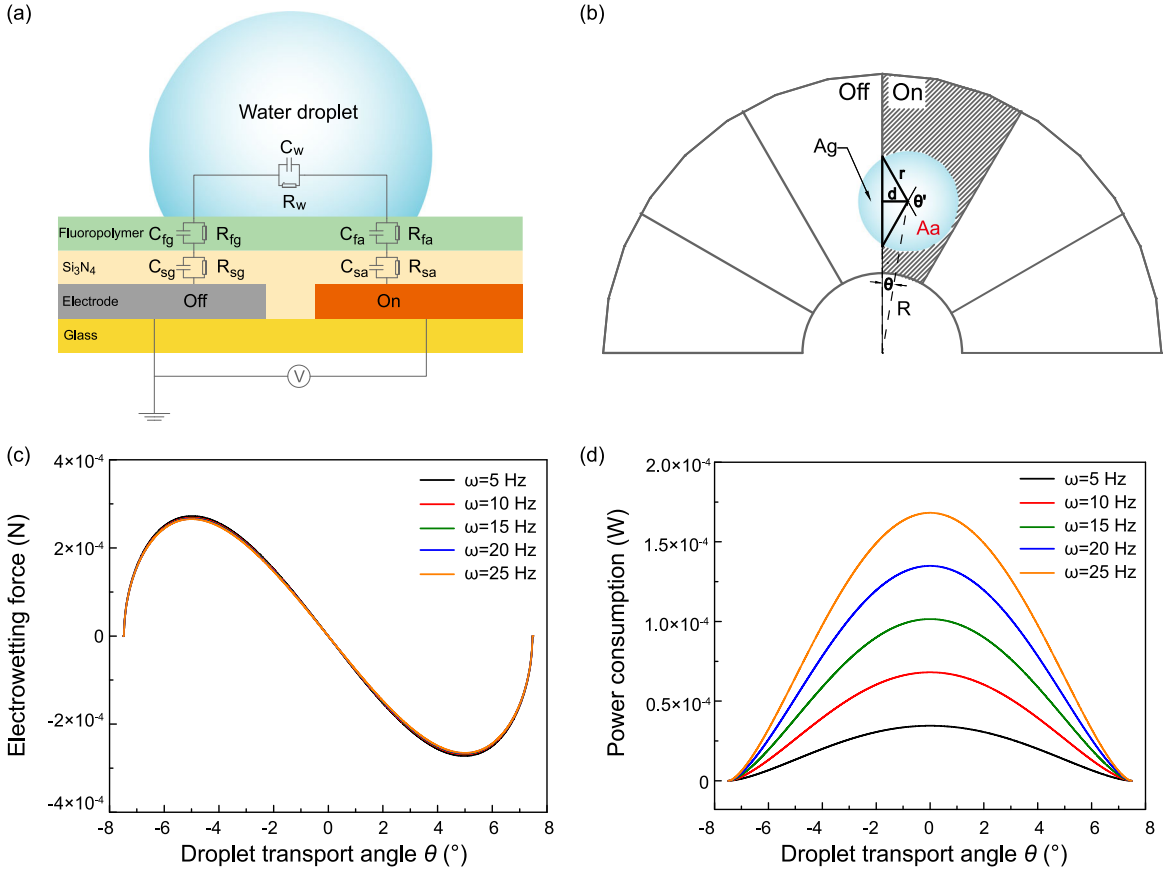

Fig. 2 Electrowetting force analysis via lumped-parameter method. a Side view and **b** top view of a droplet straddling two electrodes with an applied potential difference. The whole electrowetting on dielectric (EWOD) system can be considered as a resistor-capacitor (RC) circuit network for EWOD force analysis. For simplicity, the effect of interdigitated teeth structures along the radial edges of each electrode is ignored in this analysis. **c** EWOD driving force versus droplet transport angle θ. **d** EWOD system power consumption versus droplet transport angle θ.

$F_{EWOD} = \frac{dE(\theta)}{d\theta}$. The EWOD driving force on the droplet and the power consumption are plotted against the position angle θ in Fig. 2c, d, respectively. As the fan angle of each electrode sector is 15°, Fig. 2c, d are plotted in the range of −7.5° to 7.5°, corresponding to a full step of the droplet movement.

As shown in Fig. 2c, the RC network analysis indicates that (1) the magnitude of EWOD driving force is in the order of hundreds of μN; (2) the EWOD force is always directed toward the central gap between the two straddled electrode units; and (3) the magnitude of EWOD force barely changes with the low AC frequencies (<25 Hz). From Fig. 2d, it can be concluded that (1) the power consumption of the EWOD system increases with increasing AC frequency; (2) the magnitude of the power consumption is in the order of $\sim 10^{-5} - 10^{-4}$ W; and (3) the maximum power consumption during each step of droplet actuation happens at the central gap between the two straddled electrode units. This RC network analysis elucidates the observed droplet movement characteristics actuated by EWOD and the power consumption of the EWOD system.

To calculate the required driving force to rotate the membrane reflector, we denote the inner diameter of the hub as d_1, the outer diameter of the hub as d_2, the distance between the droplet and the axis of the shaft as R, the moment of inertia of the hub as J_{hub}, and the torque induced by the rotational friction between the shaft and the hub as τ_f. As the droplet drags the reflecting membrane, which is attached to the hub, the rotation angle of the hub is equal to the droplet position angle θ. Assuming the moment of inertia of the thin reflector membrane is negligible, we can apply the following governing equation for the rotation of the hub:

$$J_{hub}\ddot{\theta} + \tau_f - F_{droplet}R = 0 \quad (4)$$

where $F_{droplet}$ is the driving force on the reflector exerted by the water droplet. The friction torque τ_f can be derived from the following:

$$\tau_f = \int_0^{2\pi} \frac{F_f d_1}{2} d\theta \quad (5)$$

where $F_f = \xi G$ is the friction between the shaft and the rotation hub, $\xi \approx 0.1$ is the friction coefficient between the steel shaft and the ceramic hub (Supplementary Note 3)[33], and G is the gravity of the rotary hub and the reflector membrane. Combining Eqs. (4) and (5), we estimated the required minimum driving force exerted by the EWOD-actuated droplet on the membrane reflector as $F_{droplet} \approx 2.5 \times 10^{-5}$ N.

The other resistant force owing to the pinning force between the droplet and the EWOD platform can be scaled as:

$$F_{liquid-solid} \sim \pi r\gamma(\cos\theta_{adv} - \cos\theta_{rec}) \quad (6)$$

where $\gamma = 0.072$ N m^{-1} is surface tension of water, $r = 3$ mm is the droplet radius, $\theta_{adv} \approx 130°$ is the droplet advancing contact angle owing to electrowetting, $\theta_{rec} \approx 105°$ is the droplet receding contact angle on the substrate. Substituting these parameter values into Eq. (6), the droplet-substrate friction force $F_{liquid-solid} \approx 1 \times 10^{-5}$ N. As the EWOD driving force F_{EWOD} from the droplet can be as high as 3×10^{-4} N, which is an order of magnitude higher than the force needed to rotate the hub (i.e.,

$F_{EWOD} \gg F_{droplet} + F_{liquid-solid}$), we are certain that the EWOD-actuated water droplet can facilely drive the reflection plate toward the specific orientation as desired.

Steering speed, range, and insertion loss. The EWOD rotary steering system was assembled after the fabrication of each component such as the EWOD platform and the superlattice rotary hub. Then, the steering speed and range of the EWOD-driven reflecting membrane were tested on this EWOD rotary system. As water is one of the most widely used electrowetting fluids, we adopted deionized (DI) water in this work for demonstrating the feasibility of actuating a macroscale reflecting membrane by a liquid microdroplet as the proof of concept. To slow down the evaporation process of a water droplet, a proper amount of glycerol can be added in to water to form glycerol–water mixture. For practical applications, ionic liquids are good alternatives owing to their extremely low vapor pressure (as low as ~10^{-12} mm Hg), negligible evaporation rate, and high electrical conductivity[34]. Fig. 3a shows the setup of the EWOD beam steering system, including the annular array of EWOD control electrodes, the superlattice rotary hub, the membrane reflector, and a DI water droplet as the actuation medium. The assembled rotary device has the dimension of 5 cm × 7.5 cm × 2.5 cm, which can be made more compact by further condensing electrode elements and leads. In the open-plate configuration of EWOD, the footprint of the droplet is required to span at least three electrode units so that the droplet can be continuously actuated forward[31]. According to this actuation criterion and the electrode unit size, a DI water droplet of ~50 μL was adopted by us for EWOD actuation. A square-wave AC voltage of 40 V_{AC} with a low frequency of 20 Hz was applied to actuate the droplet while preventing dielectric layer polarization. The droplet was consecutively driven forward by successively powering the electrode elements under the leading edge of the droplet. For beam steering purpose, the droplet was attached to the reflector and dragged the reflector to rotate to the desired orientation via the digital actuations of EWOD, as illustrated in Fig. 3b and Supplementary Movie 1. By sequentially turning on the electrode units in a clockwise direction, the whole rotating (steering) process of the reflection plate was captured by a camera (Canon VIXIA HF R700) as shown in Supplementary Movie 2.

The real time steering speed was obtained by post image processing of the captured movie. Assuming the initial orientation of the reflection plate is 0° at $t = 0$ s, Fig. 3c–f show the time-lapse snapshots of the droplet with the reflecting membrane in four different orientations owing to the EWOD digital actuations. Accordingly, Fig. 3g displays both the angular velocity and the linear velocity of the membrane corresponding to the synchronized input square-wave AC signal. The experimental results show that (1) the reflector can be stepwise tuned with a pace of 15° in each EWOD actuation, which is mainly contingent on the electrode element fan angle; (2) the actuation manner of the droplet and hence the reflecting membrane is pulse-like with the maximum transient angular steering velocity as high as 353.5° s^{-1} (the maximum droplet linear velocity is 33.9 mm s^{-1}) and the average angular steering velocity during a full circle of trail is ~21.7° s^{-1}; (3) the dynamic response of the droplet lags behind the input AC signal ~ 0.02 s because of the droplet inertia; and (4) the EWOD rotary device enables 360° lateral steering of the reflector around the shaft without contact angle saturation effect. It is noteworthy that the water droplet oscillates in response to the AC input signals during each step of EWOD actuations. Such droplet oscillations can be effectively mitigated by applying a higher frequency AC voltage in EWOD with compromised power consumption. The angular steering resolution can be further improved by designing finer electrode elements with a smaller sector angle, i.e., <15°.

Another vital factor of a beam steering system is the insertion loss of the system. Insertion loss is the signal power loss that arises as a result of inserting a certain device (e.g., reflecting membrane) in to the signal transmission path[35]. Mathematically, it is the logarithmic ratio of the power entering, P_{in}, to the power coming out of the beam steering system, P_{out}, expressed in dB:

$$Insertion\ loss(dB) = 10log\frac{P_{in}}{P_{out}} \quad (7)$$

Any beam steering system with substantial amount of transmission power loss can significantly degrade the overall performance of the system. Furthermore, lower insertion loss implies lower energy requirements, leading to enhanced energy efficiency of the system. The signal transmission performance of our EWOD rotary system mainly depends on the specular reflectance of the reflecting membrane (3 M Vikuiti enhanced specular reflector). In order to prevent the droplet spreading over the reflecting membrane, the reflecting membrane was coated with a thin hydrophobic layer of fluoropolymer (FluoroPel PFC1101V-FS, Cytonix) during the experiment. The specular reflectances of the reflecting membrane with and without the fluoropolymer coating as shown in Fig. 3h were measured in a broadband wavelength of 200 nm to 1000 nm using the spectrophotometer (Cary 5000 UV-vis-NIR).

The measured specular reflectance indicates that the optimum wavelength of this reflecting membrane is in the range of ~400–800 nm. In this optimum spectrum, the average specular reflectance of the membrane without the fluoropolymer coating $\bar{\wp}_{no\ coating}$ can reach as high as 98.2%. In comparison, the average specular reflectance of the membrane with coating $\bar{\wp}_{coating}$ is ~86.8%. Therefore, the reflecting membrane without any coating has a superb intrinsic reflectance, whereas the hydrophobic coating slightly degrades the specular reflectance of the reflector. It is thus concluded that the insertion loss of this rotary EWOD beam steering system is ~1.5 dB in the broadband spectrum of 400–800 nm. To have a better performance of signal transmission and even lower insertion loss, we can apply a thinner coating of fluoropolymer on a high specular reflectance membrane or make a hydrophobic–hydrophilic hybrid surface treatment.

Optical beam tuning tests. Based on the EWOD rotary device, we conducted beam steering tests by adaptively redirecting an incident laser beam to the target photodetectors located at three different directions, as shown in Fig. 4a. The red laser beam with an intensity of 1.18 mW at $\lambda = 635$ nm was adopted as the signal source. Three photodiodes, i.e., PD1 (ThorLab DET100A), PD2, and PD3 (ThorLab S120c), were used as the signal detectors with the aperture size of 9.5 mm in diameter and the light detecting resolution of 0.001 mW, and they were placed 25 cm away from the EWOD rotary hub at the directions of 96°, 127°, and 221°, respectively (the incident direction of the laser beam was set as 0°). To deduct the ambient light influence, the three photodetectors were first calibrated to filter out the effect of the background light. The reflecting membrane in contact with the droplet was tuned clockwise to steer the incident beam to PD1, PD2, and PD3 in sequence. The illumination lasted for ~1 s on each receiver, as reflected by the three pulses in Fig. 4b. Driven by the square-wave AC voltage (40 V_{AC}, 20 Hz), the EWOD rotary system fulfilled the desired beam steering via adaptively modulating the orientations of the rotating membrane.

In general, the main quantities defining the performance of a liquid-based beam steering system are the maximum steering angle, the maximum steering angular velocity, and the magnitude

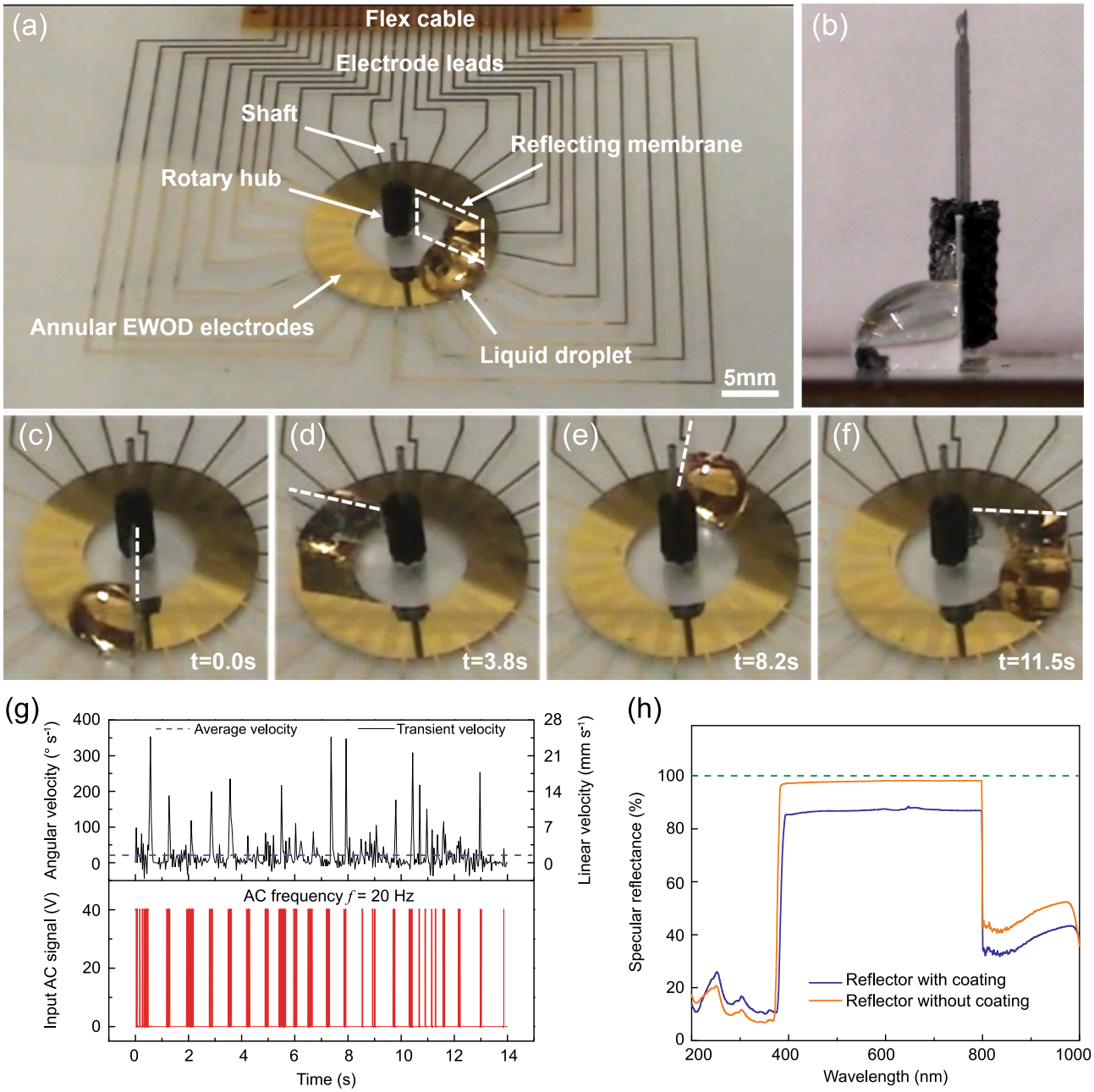

Fig. 3 Experimental test of rotary electrowetting on dielectric (EWOD) beam steering system. a Rotary electrowetting on dielectric (EWOD) beam steering system. The dashed white parallelogram indicates the reflecting membrane. **b** Side view of the droplet adhered to the reflecting membrane. **c**–**f** The snapshots of the reflecting membrane at different orientations. The dashed line in each snapshot indicates the top edge of the reflecting membrane. **g** Steering speed of the reflecting membrane driven by EWOD in response to the intermittent and synchronized square-wave alternating current (AC) signals. The dashed line indicates the average angular velocity and the average linear velocity. **h** Experimentally measured specular reflectance of the reflecting membrane with and without the fluoropolymer coating.

of actuation voltage (or power consumption). The experimental results of our EWOD rotary beam steering system are compared with the state-of-the-art liquid-based beam steering devices as shown in Table 1. (Herein, the aperture size in a beam steering system refers to the effective area for receiving the incident optical beam. In this work, the aperture size is the area of the reflecting membrane that can be modified according to various application requirements.) Our rotary EWOD system is unique and provides outstanding performance over the existing liquid-based beam steering systems, most of which are based on light refraction to achieve beam steering with a relatively high insertion signal loss, a high actuation voltage, a limited steering range and steering speed. The main merits of our rotary EWOD system are summarized as (1) The rotary EWOD actuation mechanism is integrated with a low friction superlattice hub to achieve adaptive beam steering by reflection with low insertion loss. In contrast to beam steering by light refraction, the beam steering by tuning the reflecting membrane orientation via EWOD can significantly mitigate the dispersion and aberration of optical signals during transmission, leading to an insertion loss as low as ~1.5 dB. (2) Innovative rotary electrodes are designed for EWOD actuation and hence hub rotation with a large beam steering range. The annulus-shaped EWOD electrodes enables the reflecting membrane fulfill a full loop of rotation without the limitation of

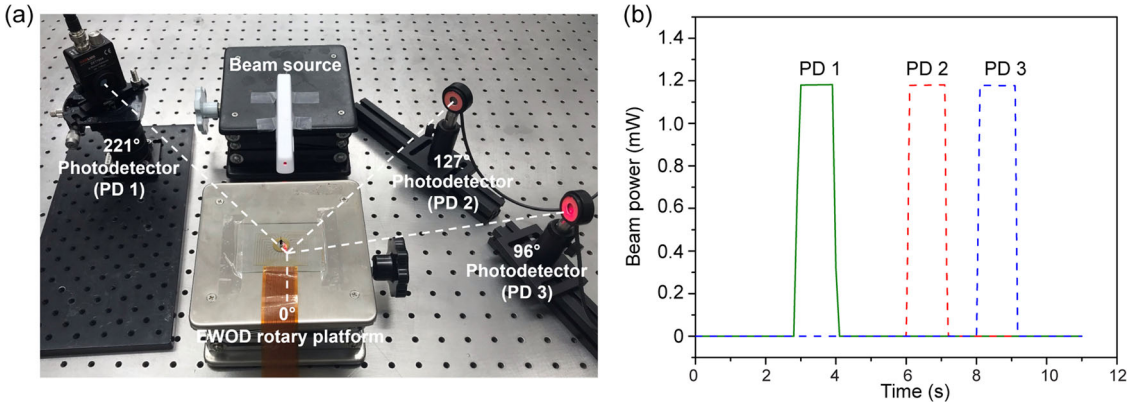

Fig. 4 Optical beam steering tests. a Beam steering setup based on the rotary electrowetting on dielectric (EWOD) platform. **b** Steered beam signals detected by the three distributed photodiode receivers.

Table 1 Comparison with the state-of-the-art liquid-based beam steering devices.

Reference	Working principle	Steering range (°)	Max steering speed (°/s)	Voltage requiring (V)	Aperture size (mm)
Cheng et al.[16]	Electrowetting	0 ~ 15	2.3	44	10 by 10
Lin et al.[19]	Dielectrophoresis	± 0.87	—	180	15 by 15
Liu et al.[21]	Electrowetting	± 30	16.8	65	3.6 by 3.6
Luo et al.[18]	Electrowetting	0 ~ 22.3	63.7	90	4 by 4
Kim et al.[20]	Dielectrowetting	± 22.7	—	450	—
This work	EWOD	0 ~ 360	353.5	40	6 by 6

contact angle saturation[23]. So far, there is no other liquid-based beam steering systems that can achieve 360° full-range beam steering as this work. (3) Optimum design of the electrode shape, size, and gap, and the dielectric layer thickness leads to low actuation voltage and power consumption. By comparing the droplet actuation performances with different dielectric layer materials and various designs of the electrode unit, the rotary EWOD system is optimally designed using the trapezoid electrode unit with interdigitated teeth (Supplementary Fig. 1b) and using Si_3N_4 as the dielectric layer, leading to a low actuation voltage of 40 V_{AC} and a low power consumption on the order of ~10^{-5}–10^{-4} W.

Discussion

Beam steering is a widely investigated and used technology in optics, RF/microwave transmission and wireless communications[36,37]. In recent years, there has been a resurgent interest in this area because of the demanding needs from many critical future photonics applications such as lidar for automated driving and 3D sensing for virtual reality (VR). As such, there have appeared numerous techniques to solve the problems associated with current beam steering schemes based on bulk optics[38–41]. However, most of these schemes still suffer from limited angular range, low speed and high optical loss, in contrast to the standard bulk-optic solutions that can cover almost all angles with very low loss.

In this work, we demonstrate an adaptive optical beam steering system based on the digital operations of an EWOD-driven fluidic rotor. Compared with other liquid-based beam steering devices, the EWOD rotary platform integrated with the 3D printed superlattice hub endows the system with the widest lateral steering range (360°), the fastest response (~353.5° s^{-1}), the lowest voltage requirement (~40 V), and the lowest power consumption (~10^{-5} W). Via the specular reflection mode of beam steering, there is no optical aberration incurred during the beam transmission. Importantly, the full-range steering is not constrained by the contact angle saturation effect of EWOD, which generally plays an inextricable role in conventional EWOD systems. Actually, by integrating EWOD-controlled liquid prism in to the system, the beam can be guided not only laterally but also omnidirectionally.

Moreover, the employment of this high-performance EWOD-controlled fluidic rotor instead of the conventional motor-driven techniques will facilitate the next-generation development of reconfigurable electronic systems[42,43] and optical switching systems (as shown in Supplementary Fig. 2 and Supplementary Note 4) with high adaptability. As such, this EWOD-driven beam steering system can be used for photonic synthetic aperture radar (SAR)[44,45] applications. The typical setup of photonic SAR systems requires the steering of the optical beam around the target. Owing to the bulky setup of the state-of-the-art photonic systems, it is very difficult to achieve this goal using conventional optical components and schemes. Inspiringly, the compact EWOD beam steering devices can be easily integrated into the photonic SAR system to achieve adaptive optical beam steering for photonic SAR measurements. Therefore, it is our belief that this EWOD-based work could contribute to the photonics community by offering an alternative solution to beam steering.

Methods

Fabrication of rotary EWOD substrate. This rotary EWOD platform fabrication process mainly includes the following sequential steps: electrode array deposition, dielectric layer coating, hydrophobic layer spin-coating, and flex cable attachment. The annular array of EWOD electrodes were fabricated on a glass slide (Corning 26005, Ted Pella). First, a thin layer of S1813 photoresist (Dow Electronic Materials MICROPOSIT) was spin-coated on the glass substrate, and then the photoresist layer was hardened by soft baking at 115 °C for 1 min. Next, the annular array of electrodes was patterned in the photoresist by exposing UV light through the electrode mask in a photolithography system (Karl Süss MA6). Thus, the electrode

pattern was presented by dipping the substrate into the developer solution (AZ 400 K). After patterning the electrode array via photolithography, the three layers of 5-nm-thick Ti, 120-nm-thick Au, and 5-nm-thick Ti were successively deposited on the patterned substrate using electron beam evaporation (Kurt J. Lesker PVD 250). A 120-nm-thick Si_3N_4 dielectric layer was subsequently deposited on the top of the electrode array by PECVD (Trion Orion III). With a low deposition rate of 49 nm/min, the chemical vapor deposition process can effectively mitigate the formation of pinholes in the dielectric layer, which would otherwise lead to undesired liquid electrolysis during EWOD operations. Then, a 50-nm-thick fluoropolymer (FluoroPel PFC1101V-FS, Cytonix) was spin-coated on the dielectric layer. The hydrophobic coating gives rise to a larger contact angle of ~112° for the water droplet and smaller contact friction, which is desirable for EWOD droplet manipulation. Finally, the 24 leads of the electrodes were bonded with the flex cable using a hot bar soldering system (PHM 1-1, Fancort Industries). For EWOD operations, the EWOD rotary device was connected to a custom-designed, multi-channel controller, which provides 0–50 V of DC/AC voltages on 128 channels[31].

Data availability

All essential data are available in the manuscript. Additional data are given in Supplementary Table 1. Further supporting data can be provided from the corresponding author upon request.

Received: 10 June 2019; Accepted: 7 January 2020;
Published online: 27 January 2020

References

1. Jia, H. et al. WDM-compatible multimode optical switching system-on-chip. *Nanophotonics* **8**, 889–898 (2019).
2. Zhang, C. et al. Self-powered optical switch based on triboelectrification-triggered liquid crystal alignment for wireless sensing. *Adv. Funct. Mater.* **29**, 1808633 (2019).
3. Blanche, P.-A., LaComb, L., Wang, Y. & Wu, M. Diffraction-based optical switching with MEMS. *Appl. Sci.* **7**, 411 (2017).
4. Peralta, J. O. & de Peralta, M. T. C. Security PIDS with physical sensors, real-time pattern recognition, and continuous patrol. *IEEE Trans. Syst. Man Cybern. Part C Appl. Rev.* **32**, 340–346 (2002).
5. Guo, N., Qiu, R. C., Mo, S. S. & Takahashi, K. 60-GHz millimeter-wave radio: principle, technology, and new results. *EURASIP J. Wirel. Commun. Netw.* **2007**, 48–48 (2007).
6. Li, M., Dempster, A. G., Balaei, A. T., Rizos, C. & Wang, F. Switchable beam steering/null steering algorithm for CW interference mitigation in GPS C/A code receivers. *IEEE Trans. Aerosp. Electron. Syst.* **47**, 1564–1579 (2011).
7. Heck, M. J. Highly integrated optical phased arrays: photonic integrated circuits for optical beam shaping and beam steering. *Nanophotonics* **6**, 93 (2017).
8. Cheng, J.-T. & Chen, C.-L. Active thermal management of on-chip hot spots using EWOD-driven droplet microfluidics. *Exp. Fluids* **49**, 1349–1357 (2010).
9. Gong, J. All-electronic droplet generation on-chip with real-time feedback control for EWOD digital microfluidics. *Lab. Chip* **8**, 898–906 (2008).
10. Nelson, W. C. & Kim, C.-J. Droplet actuation by electrowetting-on-dielectric (EWOD): a review. *J. Adhes. Sci. Technol.* **26**, 1747–1771 (2012).
11. Lee, J., Moon, H., Fowler, J., Schoellhammer, T. & Kim, C.-J. Electrowetting and electrowetting-on-dielectric for microscale liquid handling. *Sens. Actuat. A Phys.* **95**, 259–268 (2002).
12. Reza, S. A. & Riza, N. A. A liquid lens-based broadband variable fiber optical attenuator. *Opt. Commun.* **282**, 1298–1303 (2009).
13. Smith, N. R., Abeysinghe, D. C., Haus, J. W. & Heikenfeld, J. Agile wide-angle beam steering with electrowetting microprisms. *Opt. Express* **14**, 6557–6563 (2006).
14. Hou, L., Smith, N. & Heikenfeld, J. Electrowetting manipulation of any optical film. *Appl. Phys. Lett.* **90**, 251114 (2007).
15. Takei, A., Matsumoto, K. & Shomoyama, I. Capillary motor driven by electrowetting. *Lab. Chip* **10**, 1781–1786 (2010).
16. Cheng, J.-T. & Chen, C.-L. Adaptive beam tracking and steering via electrowetting-controlled liquid prism. *Appl. Phys. Lett.* **99**, 191108 (2011).
17. Cheng, J.-T., Park, S. & Chen, C.-L. Optofluidic solar concentrators using electrowetting tracking: concept, design, and characterization. *Sol. Energy* **89**, 152–161 (2013).
18. Luo, L., Li, L., Wang, J.-H., Yuan, R.-Y. & Wang, Q.-H. Liquid prism with dual-interface based on electrowetting effect. *Opt. Commun.* **425**, 180–184 (2018).
19. Lin, Y.-J., Chen, K.-M. & Wu, S.-T. Broadband and polarization-independent beam steering using dielectrophoresis-tilted prism. *Opt. Express* **17**, 8651–8656 (2009).
20. Kim, D., Park, Y., Lee, D. Y. & Chung, S. K. in *2018 IEEE Micro Electro Mechanical Systems (MEMS)* 585–587 (IEEE, Belfast, 2018).
21. Liu, C., Wang, Q.-H. & Wang, M.-H. Mirror reflector actuated by liquid droplet. *IEEE Photonics Technol. Lett.* **26**, 1077–1080 (2014).
22. Zheng, X. et al. Ultralight, ultrastiff mechanical metamaterials. *Science* **344**, 1373–1377 (2014).
23. Peykov, V., Quinn, A. & Ralston, J. Electrowetting: a model for contact-angle saturation. *Colloid Polym. Sci.* **278**, 789–793 (2000).
24. Quinn, A., Sedev, R. & Ralston, J. Contact angle saturation in electrowetting. *J. Phys. Chem. B* **109**, 6268–6275 (2005).
25. Mugele, F. Fundamental challenges in electrowetting: from equilibrium shapes to contact angle saturation and drop dynamics. *Soft Matter* **5**, 3377–3384 (2009).
26. Deshpande, V. S., Fleck, N. A. & Ashby, M. F. Effective properties of the octet-truss lattice material. *J. Mech. Phys. Solids* **49**, 1747–1769 (2001).
27. Zheng, X. et al. Multiscale metallic metamaterials. *Nat. Mater.* **15**, 1100 (2016).
28. Cui, H., Hensleigh, R., Chen, H. & Zheng, X. Additive Manufacturing and size-dependent mechanical properties of three-dimensional microarchitected, high-temperature ceramic metamaterials. *J. Mater. Res.* **33**, 360–371 (2018).
29. Hensleigh, R. M. et al. Additive manufacturing of complex micro-architected graphene aerogels. *Mater. Horiz.* **5**, 1035–1041 (2018).
30. Dong, L., Deshpande, V. & Wadley, H. Mechanical response of Ti–6Al–4V octet-truss lattice structures. *Int. J. Solids Struct.* **60**, 107–124 (2015).
31. Cheng, J.-T. & Chen, C. L. Adaptive chip cooling using electrowetting on coplanar control electrodes. *Nanosc. Microsc. Thermo. E* **14**, 63–74 (2010).
32. Mugele, F. & Baret, J.-C. Electrowetting: from basics to applications. *J. Phys. Condens. Matter* **17**, R705–R774 (2005).
33. Wakuda, M., Yamauchi, Y., Kanzaki, S. & Yasuda, Y. Effect of surface texturing on friction reduction between ceramic and steel materials under lubricated sliding contact. *Wear* **254**, 356–363 (2003).
34. Rogers, R. D. & Seddon, K. R. Ionic liquids–solvents of the future? *Science* **302**, 792–793 (2003).
35. Uchendu, I. & Kelly, J. R. Survey of beam steering techniques available for millimeter wave applications. *Prog. Electromagn. Res.* **68**, 35–54 (2016).
36. Sun, Y., Zheng, Z., Cheng, J.-T. & Liu, J. W. Graphene surface plasmon waveguides incorporating high-index dielectric ridges for single mode transmission. *Opt. Commun.* **328**, 124–128 (2014).
37. Zhang, M., Cheng, W. F., Zheng, Z., Cheng, J.-T. & Liu, J. S. Meridian whispering gallery modes sensing in a sessile microdroplet on micro/nanostructured superhydrophobic chip surfaces. *Microfluid Nanofluid* **23**, 106 (2019).
38. Kurosaka, Y. et al. On-chip beam-steering photonic-crystal lasers. *Nat. Photonics* **4**, 447 (2010).
39. Sun, J., Timurdogan, E., Yaacobi, A., Hosseini, E. S. & Watts, M. R. Large-scale nanophotonic phased array. *Nature* **493**, 195 (2013).
40. Hutchison, D. N. et al. High-resolution aliasing-free optical beam steering. *Optica* **3**, 887–890 (2016).
41. Wu, P. C. et al. Dynamic beam steering with all-dielectric electro-optic III–V multiple-quantum-well metasurfaces. *Nat. Commun.* **10**, 1–9 (2019).
42. Min, X., Bao, C. & Kim, W. S. Additively manufactured digital microfluidic platforms for ion-selective sensing. *ACS Sens.* **4**, 918–923 (2019).
43. Moazami, E., Perry, J. M., Soffer, G., Husser, M. C. & Shih, S. C. Integration of world-to-chip interfaces with digital microfluidics for bacterial transformation and enzymatic assays. *Anal. Chem.* **91**, 5159–5168 (2019).
44. Li, R. et al. Demonstration of a microwave photonic synthetic aperture radar based on photonic-assisted signal generation and stretch processing. *Opt. Express* **25**, 14334–14340 (2017).
45. Beck, S. M. et al. Synthetic-aperture imaging laser radar: laboratory demonstration and signal processing. *Appl. Opt.* **44**, 7621–7629 (2005).

Acknowledgements

This work was funded by NSF ECCS grant #1550749. We appreciate the UT Dallas cleanroom for the mask design and fabrication.

Author contributions

J.C. and H.Z. conceived the idea and supervised the project. T.Z. and B.G. designed the EWOD masks. W.C. fabricated rotary EWOD beam steering system, analyzed the EWOD driving force and power consumption, conducted the beam steering experiments under the supervision of J.C., J.L. and Z.Z. H.C. fabricated the superlattice rotary hub, assembled the rotating components with the EWOD platform, and analyzed the rotating friction under the supervision of X.Z. X.H. assembled the EWOD devices. B.Z. tested the EWOD rotor system under the supervision of H.Z. All authors proofread the paper, made comments, and approved the manuscript.

Competing interests
The authors declare no competing interests.

Additional information
Supplementary information is available for this paper at https://doi.org/10.1038/s42005-020-0294-6.

Correspondence and requests for materials should be addressed to J.C.

Reprints and permission information is available at http://www.nature.com/reprints

Publisher's note Springer Nature remains neutral with regard to jurisdictional claims in published maps and institutional affiliations.